Journal of ELECTRONIC MATERIALS, Vol. 47, No. 1, 2018
DOI: 10.1007/s11664-017-5839-4

Influence of Europium Doping on Various Electrical Properties of Low-Temperature Sintered $0.5Ba_{0.90}Ca_{0.10}TiO_3$-$0.5BaTi_{0.88}Zr_{0.12}O_3$-0.1%CuO-$x$Eu Lead-Free Ceramics

YONGSHANG TIAN,[1,2,4,5] SHUIYUN LI,[1] SHULIN SUN,[1] YANSHENG GONG,[3] TIANTIAN LI,[1,2] YONGSHANG YU,[1,2] and QIANGSHAN JING[1,2]

1.—College of Chemistry and Chemical Engineering, Xinyang Normal University, Xinyang 464000, People's Republic of China. 2.—Henan Province Key Laboratory of Utilization of Non-metallic Mineral in the South of Henan, Xinyang 464000, People's Republic of China. 3.—Faculty of Material Science and Chemistry, China University of Geosciences, Wuhan 430074, People's Republic of China. 4.—e-mail: tianyongshang423@163.com. 5.—e-mail: tianyongshang@xynu.edu.cn

$0.5Ba_{0.90}Ca_{0.10}TiO_3$-$0.5BaTi_{0.88}Zr_{0.12}O_3$-0.1%CuO-$x$Eu (BCT-BZT-Cu-$x$Eu; x = 0–0.90%) lead-free ceramics were sintered at 1220°C with as-synthesized nanoparticles by a modified Pechini method. The structural characteristics and electrical properties of the ceramics that were influenced by varying europium-doping were investigated. All the ceramics featured high densification (relative density: ~ 96%). X-ray powder diffraction results indicated the samples possessed pure orthorhombic phase. The maximum relative permittivity (ε_r, 10869) was found at x around 0.30%. Europium ions could dope on different substitution sites in the ABO_3 lattice, which evidently influenced electrical properties with various volumes of oxygen vacancy. Moreover, the formation mechanisms of oxygen vacancy and defect electron complexes were stated. The piezoelectric properties were impacted by defect electron complexes, internal stress, ionic electronegativity, etc. The optimal electrical properties, i.e., d_{33} = 384 pC/N, Q_m = 92, and k_p = 0.36, were detected at x = 0.45%.

Key words: BCZT ceramics, europium-doped, oxygen vacancy, defect electron complexes, electrical properties

INTRODUCTION

In recent decades, lead-based piezoelectric materials have been restricted to applications in the electronic industry because of environmental pollution, though they possess prominent electrical properties.[1,2] Thus, it is urgently important to find promising lead-free candidates for replacing lead-based materials in the devices for actuators, memory storage, sensors, etc.[2] Among the lead-free candidates, calcium and zirconate co-doped $BaTiO_3$ (BCZT) ceramics materials featured excellent piezoelectric properties (piezoelectric constant; ~ 620 pC/N) near the morphotropic phase boundary, which aroused widespread concerns.[3,4] However, BCZT ceramics materials need a high sinter temperature (~ 1450°C) and possess serious temperature instability of their electrical properties, which restrict their practical applications in the electronic ceramic industry.[5]

The electrical properties of BCZT ceramics could be tailored by doping various solutes and applying different synthesized processes.[6–14] Sintering aids, as a type of low-temperature solutes, had been used to study doping BCZT ceramics because of the

(Received June 19, 2017; accepted September 27, 2017; published online October 13, 2017)

generated liquid phase in the sintering process, resulting in decreasing sintered temperature and promoting electrical properties with the phase evolutions.[6–10] In the further study of solutes, it is of interest to research BCZT ceramics doped with rare-earth elements for their amphoteric character, which could impregnate into different sites in the perovskite (ABO_3) matrix, bringing about phase evolutions and varying electrical properties.[11–15] Particularly, europium-doped BCZT ceramics have potential excellent electrical properties.[16] It was reported that the defect electron complexes possess obvious impacts on tailoring piezoelectric materials.[17] And the defect electron complexes could be formed to compensate oxygen vacancy because of the charge balance, suggesting the electrical properties were definitely influenced by the complexes.[17,18] However, there are few studies on the mechanism of varying electrical properties of BCZT ceramics that are influenced by oxygen vacancy and defect electron complexes with various europium contents.

In this work, europium-doped $0.5Ba_{0.90}Ca_{0.10}TiO_3$-$0.5BaTi_{0.88}Zr_{0.12}O_3$-0.1%CuO ceramics were sintered at a low temperature of 1220°C with the as-prepared nanoparticles by a modified Pechini method. The formation mechanism of varying oxygen vacancy and defect electron complexes were explored. In addition, the effects of europium on dielectric frequency dispersion, diffused phase transition, dielectric properties, ferroelectric properties, and piezoelectric properties were all investigated in detail.

EXPERIMENTAL PROCEDURE

$0.5Ba_{0.90}Ca_{0.10}TiO_3$-$0.5BaTi_{0.88}Zr_{0.12}O_3$-0.1%CuO-$x$Eu (abbreviated as BCT-BZT-Cu-xEu; x = 0%, 0.15%, 0.30%, 0.45%, 0.60%, 0.75%, and 0.90%) lead-free ceramics were prepared by a modified Pechini method as in our previous report.[19,20] The starting raw materials of $Ti(OC_4H_9)_4$, $Ca(NO_3)_2$, $Ba(CH_3COO)_2$, $Zr(NO_3)_4$, $Eu(NO_3)_3$, citric acid, ethylene glycol, and ethyl alcohol were firstly synthesized as sol, and then the sol was calcined at 850°C in furnace for nanoparticles. Subsequently, the nanoparticles were stoichiometrically mixed with 0.1 mol.% CuO powders and homogeneously grounded in agate mortar. After mixing with 2.5 wt.% polyvinyl alcohol (PVA), the powders were uniaxially pressed into discs of ~ 2 mm in thickness and 18 mm in diameter under the pressure of 160 MPa for the green body, then buried in Al_2O_3 powders and sintered at the temperature of 1220°C for 5 h in the air for obtaining the ceramics. The silver electrodes were brushed on both polished samples discs surfaces by firing silver paste at the temperature of 580°C for 12 min for the later electrical properties measurements. Subsequently, the samples were polarized at 40°C by applying a direct-current (dc) electric field of 5 kV/cm for ~ 40 min in the silicone oil bath.

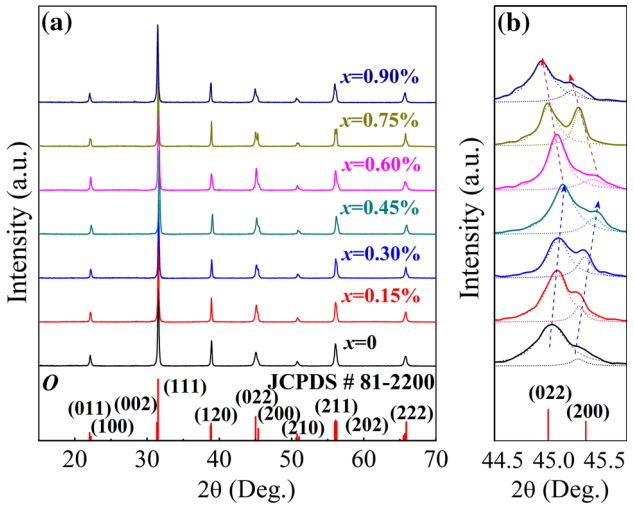

Fig. 1. (a) XRD patterns and (b) the enlarged regions (44.4°–45.9°) of the BCT-BZT-Cu-xEu ceramics doped with various europium contents (x).

The crystal structure was detected by x-ray powder diffraction (XRD; Mini Flex 600) under a scanning angle rate of 0.05°/s with Cu-Kα radiation. A dielectric measurement system (HDMS-1000V) was used to test the relative permittivity (ε_r) and loss tangent (tan δ). The polarization–electric field (P–E) hysteresis loops were determined by a radiant precision workstation (PREMER II). After the polarized process, the mechanical quality factor (Q_m) and planar vibration electromechanical coupling factors (k_p) were measured using precision impedance analyzer (Keysight 4990A). A quasistatic piezoelectric constant testing meter (ZJ-3AN) was used to measure the piezoelectric constant (d_{33}) at 25°C.

RESULTS AND DISCUSSION

Figure 1 shows the XRD patterns of the BCT-BZT-Cu-xEu ceramics doped with varying europium contents. It can be seen all the ceramics showed a typical perovskite structure (ABO_3) with orthorhombic (JCPDS # 81-2200) phase at room temperature, suggesting that europium successfully diffused into the ABO_3 lattice. From the enlarged XRD patterns in Fig. 1b, (022) and (200) diffraction peaks initially shifted to higher 2θ angles, and monotonically to lower 2θ angles with increasing addition of x, which was associated with Eu^{3+} (ionic radius 0.095 nm) firstly substituted Ca^{2+} (0.134 nm)/Ba^{2+} (0.161 nm), and then in turn to replace Zr^{4+} (0.072 nm)/Ti^{4+} (0.0605 nm) in the structure.[21,22] From Fig. 1b, the relative intensity of (022) and (200) diffraction peaks changed with increasing addition of x, showing the various degrees of crystallinity. In addition, the width of (022) and (200) diffraction peaks initially broadened and then narrowed with increasing addition of x, indicating the average grain size firstly decreased and then increased according to the Debye–Scherrer formula.[23]

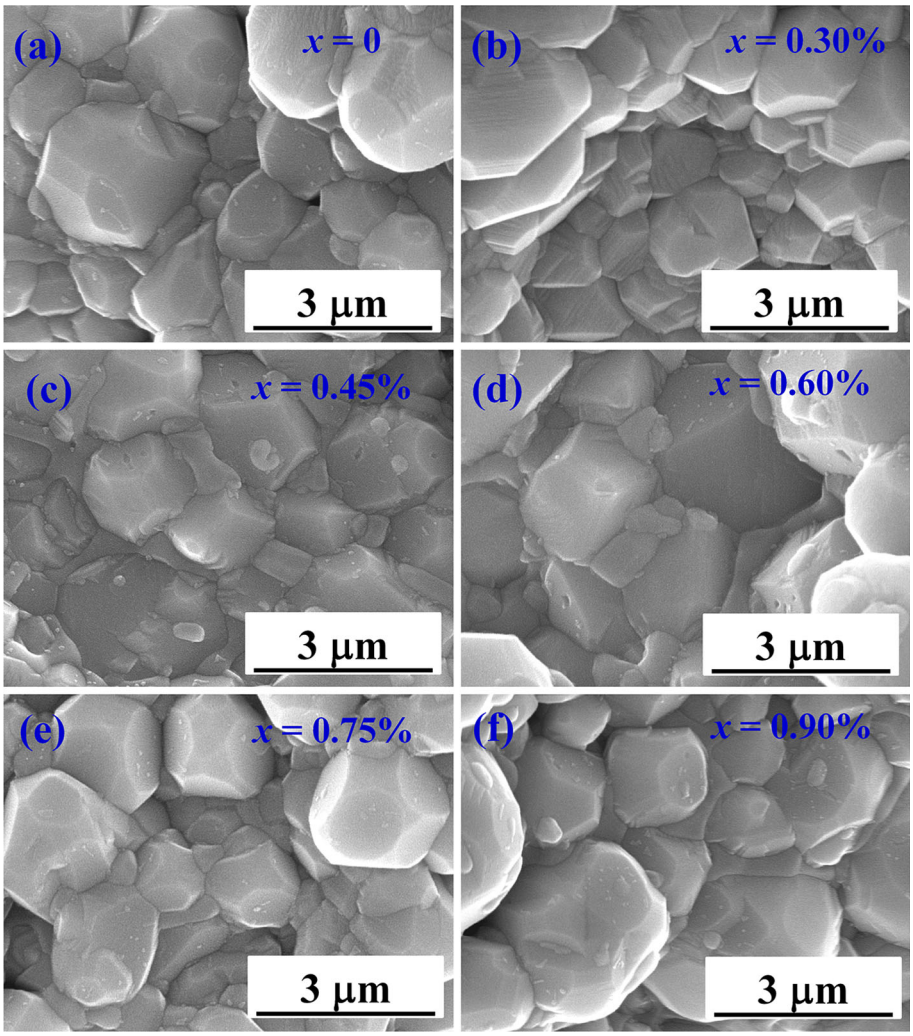

Fig. 2. SEM images of fracture surface morphology of the BCT-BZT-Cu-*x*Eu ceramics doped with europium contents (*x*) of (a) 0%, (b) 0.30%, (c) 0.45%, (d) 0.60%, (e) 0.75%, and (f) 0.90%.

Figure 2 shows SEM images of fracture surface morphology of the BCT-BZT-Cu-*x*Eu ceramics doped with europium contents of (a) 0%, (b) 0.30%, (c) 0.45%, (d) 0.60%, (e) 0.75%, and (f) 0.90%. It is found that all the samples featured a high densification with little cavity. The average grain size (G_{AV}) of the samples, estimated by the linear intercept method, firstly decreased and then elevated with increasing of x, was in line with the XRD results in Fig. 1. It was reported that the diversified grain size was mainly associated with the volume of oxygen vacancy.[24,25] That is, oxygen vacancy was a benefit for the particle diffusion in the structure during the sintering process.[24] Thus, the decreased G_{AV} was attributed to the reduced oxygen vacancy with a small addition of x, and the large abnormal grains with excessive europium contents might be derived from a large volume oxygen vacancy.[25] The formation mechanism of oxygen vacancy will be discussed as follows.

The density and relative density of the BCT-BZT-Cu-*x*Eu ceramics doped with varying europium contents are shown in Fig. 3. As can be seen, all the samples showed high densification (relative density, $\sim$ 96%), as consistent with the dense structure of SEM results in Fig. 2. The ceramics density and relative density elevated with a small addition of x, reaching up to a maximum of 5.518 g/cm^3 and 96.8%, respectively. Then, the densification of ceramics tended to decrease with further addition of x. The reasons for the decreased densification with excessive x were the fierce crystal lattice distortion and a mass of pores between large abnormal grains in the structure.

Figure 4 shows the loss tangent (tan δ) and relative permittivity (ε_r) of the BCT-BZT-Cu-*x*Eu ceramics under the dependent temperature doped with varying europium contents at 10 kHz. It can be distinctly detected there existed two peaks, corresponding to the phase transitions of orthorhombic-

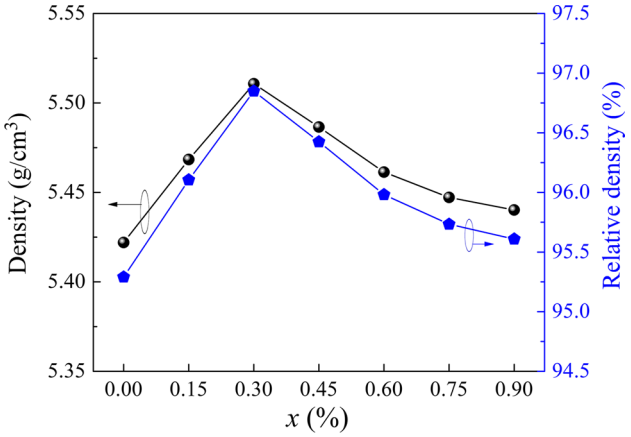

Fig. 3. The density and relative density of the BCT-BZT-Cu-xEu ceramics doped with varying europium contents (x).

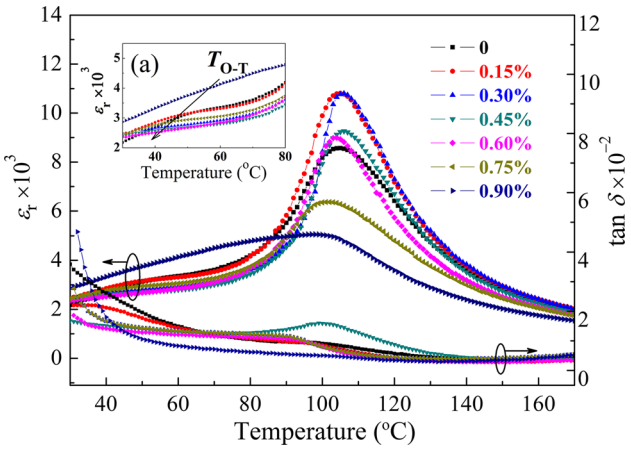

Fig. 4. The loss tangent (tan δ) and relative permittivity (ε_r) of the BCT-BZT-Cu-xEu ceramics under the dependent temperature doped with varying europium contents (x) at 10 kHz. The inset (a) displays the enlarged regions (30.1–80°C).

to-tetragonal (T_{O-T}) around 50°C and cubic–tetragonal (T_C) around 110°C, respectively. With addition of europium contents, the value of maximum ε_r around T_C elevated first, and then decreased; T_C subtly increased together with sharping dielectric peak firstly and then decreased with broadening of the dielectric peak. The maximum ε_r (10869) and T_C ($\sim$ 108°C) of the ceramics were found when x was around 0.30%, which was due to the fact that the minimum internal stress as the least volume of oxygen vacancy ($V_O^{\cdot\cdot}$) (Eq. 1) and the receded lattice distortion in the structure.[26–28] The deteriorated dielectric properties with excessive addition of x were due to the re-generated oxygen vacancy in the structure (Eq. 2). From the enlarged regions of ε_r assessed the temperature from 30.1°C to 80°C in Fig. 1b, T_{O-T} turned into a room temperature direction with a small addition of x, which could bring about the elevating piezoelectric properties.[29] Moreover, the relative low tan δ ($\sim$ 0.02) in our study was attributed to subtle flaws in the dense structure.

$$2Eu^{3+} + V_O^{\cdot\cdot} + \frac{1}{2}O_2(g) \xrightarrow{BCT-BZT-Cu} 2Eu_{Ba/ca}^{\cdot} + O_O \quad (1)$$

$$2Eu^{3+} + O_O \xrightarrow{BCT-BZT-Cu} 2Eu_{Ti/Zr}^{\prime} + V_O^{\cdot\cdot} + \frac{1}{2}O_2 \uparrow \quad (2)$$

Figure 5 shows loss tangent (tan δ) and relative permittivity (ε_r) of the BCT-BZT-Cu-xEu ceramics under the dependent temperature doped with europium contents (x) of (a) 0%, (b) 0.15%, (c) 0.30%, (d) 0.45%, (e) 0.60%, and (f) 0.75% under 100 Hz, 1 kHz, and 10 kHz. It can be seen that the dielectric frequency dispersion firstly decreased and then enhanced with more addition of x, indicating the diffused phase transition of the ceramics initially deteriorated and then enhanced.[30] The corresponding temperatures of loss tangent peaks lower than the dielectric peaks assessed various frequencies that also indicated the phase transitions, because of the orientation of dipoles needed a certain time.[30,31] With increasing the testing temperature, the value of ε_r firstly elevated ($< T_C$) and then decreased, suggesting a flabby polarization behavior for the change of dipole ordering.[32,33] In addition, the enhanced dielectric frequency dispersion and diffused phase transition of the ceramics with excessive addition of x, showing relatively inferior ferroelectric properties.[34]

In order to investigate the degree of diffused phase transition of the BCT-BZT-Cu-xEu ceramics, the Curie–Weiss law (Eq. 3) has been introduced to calculate quantitative parameters:

$$\frac{1}{\varepsilon_r} = \frac{T - T_{CW}}{C} \quad (T > T_C), \quad (3)$$

$$\Delta T_m = T_B - T_m, \quad (4)$$

where T_{CW} corresponds to the Curie–Weiss temperature; ε_r represents the relative dielectric constant; and C represents the Curie–Weiss constant. The fitted Curie–Weiss curve (Eq. 4) for inverse permittivity ($10^4/\varepsilon_r$) of the ceramics with varying temperature assessed at 10 kHz are shown in Fig. 6. As can be observed in the Fig. 6a, the temperature parameters T_m, T_B, ΔT_m, and T_{CW} represents the temperature corresponding to the maximum permittivity, the temperature when the permittivity starts to follow the Curie–Weiss law, the temperature deviation, and the Curie–Weiss temperature, respectively. All the mentioned temperature parameters above were fitted and calculated, which are all shown in Table I. The ΔT_m initially decreased from 32.6°C at x = 0–31.9°C at x = 0.30%, and then increased with further addition of x, suggesting the diffused phase transition of the ceramics firstly receded and then was enhanced. The variation of ΔT_m was associated with the local distorted

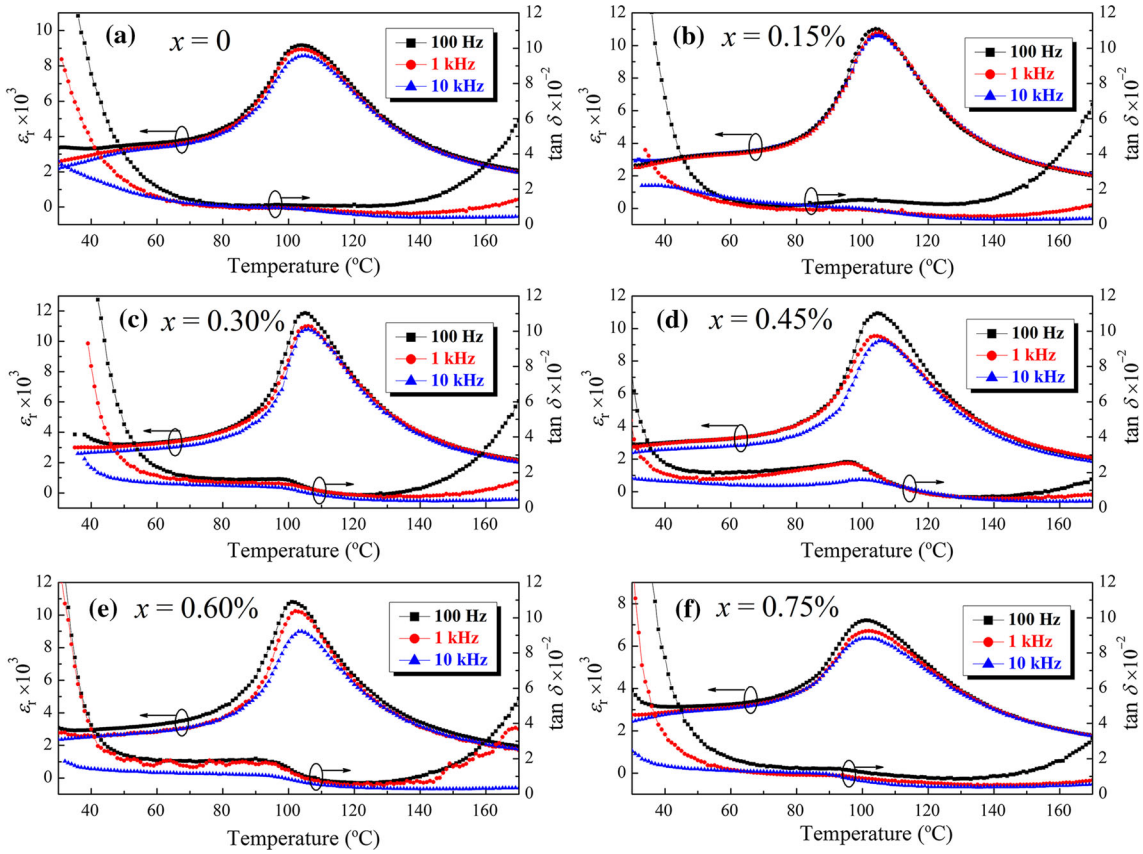

Fig. 5. The loss tangent (tan δ) and relative permittivity (ε_r) of the BCT-BZT-Cu-xEu ceramics under the dependent temperature doped with europium contents (x) of (a) 0%, (b) 0.15%, (c) 0.30%, (d) 0.45%, (e) 0.60%, and (f) 0.75% under different frequencies.

structure and imbalanced local charge.[35,36] The fitted parameters C also demonstrated the variation of diffused phase transition, which was in agreement with the result of ΔT_m. Furthermore, C featured an order of $\sim 10^5$, indicating paraelectric phase under high temperature was driven by a displacive transition.[37]

In order to further determine the degree of ferroelectric-paraelectric diffused phase transition, the modified Curie–Weiss law has been introduced to calculate quantitative parameters of the relaxation behavior (Eq. 5).

$$\ln\left(\frac{1}{\varepsilon_r}-\frac{1}{\varepsilon_m}\right)=\gamma\ln(T-T_m)-\ln C', \tag{5}$$

where γ corresponds to the degree of the diffuseness exponent that ranged from 1 (normal ferroelectric) to 2 (typical relaxor ferroelectric), and C' represents the modified Curie–Weiss constant. Parameters γ were calculated by the slope of $\ln(1/\varepsilon_r - 1/\varepsilon_m)$ versus $\ln(T - T_m)$ under 10 kHz, and are shown in Fig. 7 and Table I. It can be seen γ decreased from 1.69 to 1.48 with a small addition of x (< 0.30%), indicating the ferroelectric character of the elevated ceramic. But, γ was elevated with excessive addition of x, which might be derived from local compositional inhomogeneity in our study.[38] Besides, the deteriorated ferroelectric character with excessive addition of x was considered to be derived from a short-range motion from oxygen vacancy to $Eu'_{Ti/Zr}$, accompanying plenty of carrier migration with defect electron complexes $\left(Eu'_{Ti/Zr}-V_o^{\cdot\cdot}\right)^{\cdot}$ and $\left(3Eu'_{Ti/Zr}-V_o^{\cdot\cdot}\right)'$ (Eq. 6).[17,39,40]

$$4Eu'_{Ti/Zr}+2V_o^{\cdot\cdot}\rightleftharpoons\left(Eu'_{Ti/Zr}-V_o^{\cdot\cdot}\right)^{\cdot}+\left(3Eu'_{Ti/Zr}-V_o^{\cdot\cdot}\right)' \tag{6}$$

Figure 8 shows the BCT-BZT-Cu-xEu ceramics polarization–electric field (P–E) hysteresis loops doped with different europium contents at room temperature. It can be found all the samples featured good ferroelectric properties with the typical saturated hysteresis loop. The remnant polarization (P_r) firstly elevated and then deteriorated with increasing addition of x, which was associated with varied inter-space octahedron size, changed long-range order polarization, and a different volume of defect dipole.[41] The coercive field (E_c) decreased from 3.56 kV/cm to 1.89 kV/cm with increasing europium contents (x < 0.45%), because of the inferior pinching effects in the domain wall

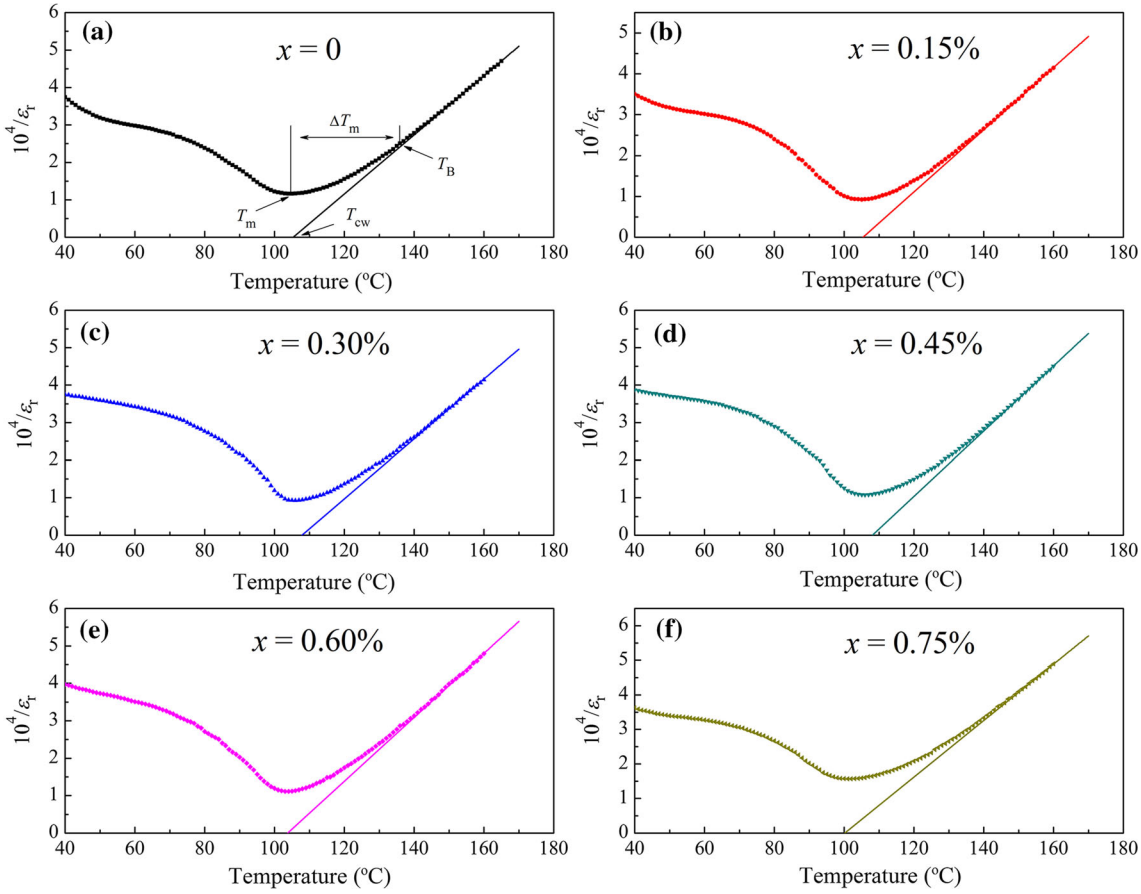

Fig. 6. Inverse permittivity ($10^4/\varepsilon_r$) of the BCT-BZT-Cu-xEu ceramics under the dependent temperature doped with europium contents (x) of (a) 0%, (b) 0.15%, (c) 0.30%, (d) 0.45%, (e) 0.60%, and (f) 0.75% assessed at 10 kHz.

Table I. Temperature of the maximum relative dielectric constant (T_m), Curie–Weiss temperature (T_{CW}), temperature of the relative dielectric constant that starts to follow the Curie–Weiss law (T_B), temperature deviation (ΔT_m), and the diffuseness exponent (γ) for the BCT-BZT-Cu-xEu ceramics doped with varying europium contents (x) measured at 10 kHz

x (%)	T_m (°C)	T_{cw} (°C)	T_B (°C)	ΔT_m (°C)	C (× 10^5°C)	γ
0	104.7	105.3	137.3	32.6	1.268	1.685
0.15	104.9	105.4	137.0	32.1	1.243	1.601
0.30	105.5	107.8	137.4	31.9	1.237	1.490
0.45	105.2	108.1	137.7	32.5	1.250	1.553
0.60	104.4	103.9	137.5	33.1	1.259	1.599
0.75	103.6	100.1	137.3	33.7	1.266	1.655
0.90	98.6	87.2	133.0	34.4	1.275	1.683

with little oxygen vacancy, weak internal stress with subtle defect structure, and little pores with dense packed microstructure,[42,43] which were consistent with the results above.

Figure 9 shows the piezoelectric constant (d_{33}), mechanical quality factor (Q_m), and planar vibration electromechanical coupling factors (k_p) of the BCT-BZT-Cu-xEu ceramics doped with varying europium contents. As can be seen, d_{33} and k_p initially elevated, and then deteriorated with more addition of x, while Q_m showed an opposite trend. The optimum electrical properties, i.e., d_{33} = 384 pC/N and k_p = 0.36 were obtained at x = 0.45%, which was attributed to the easily polarized dipole as the T_{O-T} shifted to near room temperature, resulting in complete polarization at the external

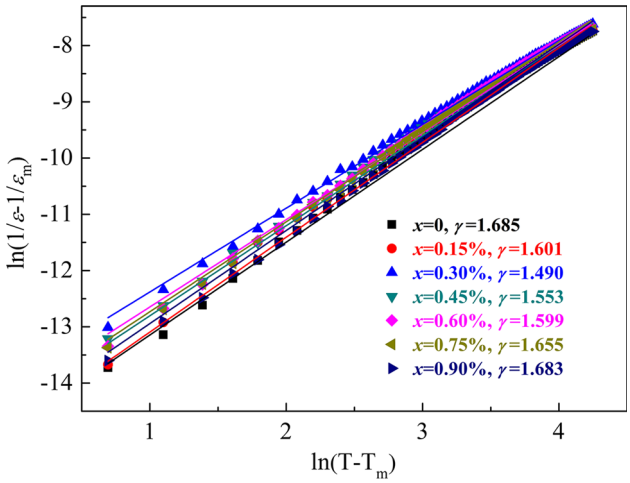

Fig. 7. The plots of $\ln(1/\varepsilon_r - 1/\varepsilon_m)$ versus $\ln(T - T_m)$ under 10 kHz for the BCT-BZT-Cu-*x*Eu ceramics doped with varying europium contents (*x*).

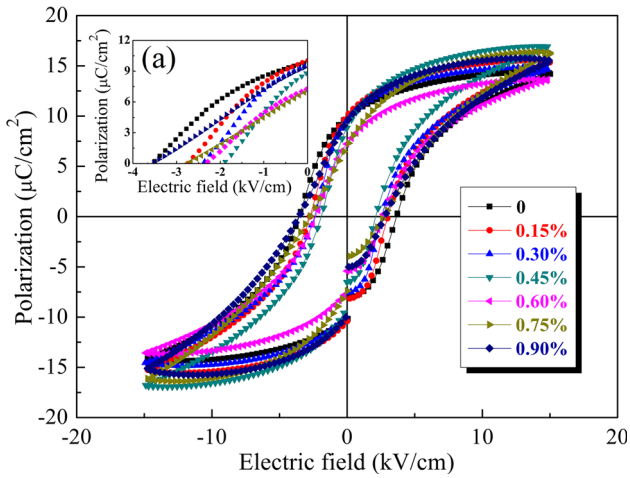

Fig. 8. The BCT-BZT-Cu-*x*Eu ceramics polarization–electric field (*P*–*E*) hysteresis loops doped with different europium contents (*x*) at room temperature. The inset (a) displays the enlarged regions (− 4 kV/cm to 0 kV/cm).

electric field.[44] The elevated piezoelectric properties with a small addition of *x* were also associated with the subtle defect structure and inferior pinching effects of the domain wall with little volume for oxygen vacancy. However, the deteriorated piezoelectric properties with excessive addition of *x* might be related to Eu^{3+} possessing a relatively lower electronegativity value (1.20) than compared with Ti^{4+} (1.54)/Zr^{4+} (1.33) in the structure, resulting in weak covalent bonds in the structure.[45] The relative low mechanical quality factor (Q_m) in our study was due to weak pinching effects in the domain wall, which was beneficial to increasing frequency bandwidth of the electron component.[46,47]

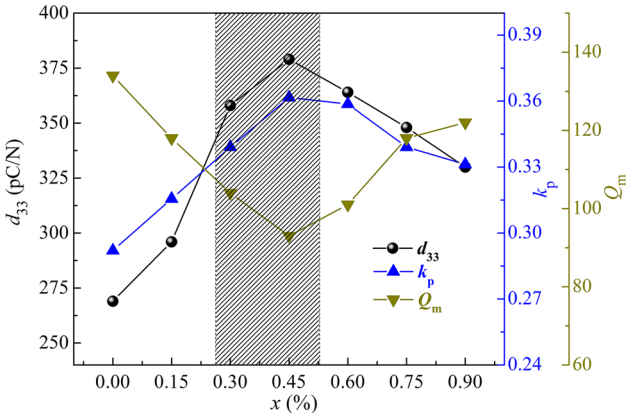

Fig. 9. The BCT-BZT-Cu-*x*Eu ceramics piezoelectric constant (d_{33}), mechanical quality factor (Q_m), and planar vibration electromechanical coupling factors (k_p) doped with varying europium contents (*x*).

CONCLUSIONS

In conclusion, the influence of europium on the structural characteristics and electrical properties of $0.5Ba_{0.90}Ca_{0.10}TiO_3$-$0.5BaTi_{0.88}Zr_{0.12}O_3$-0.1%CuO-*x*Eu ceramics that were sintered at 1220°C with as-synthesized nanoparticles by a modified Pechini method were investigated. The ceramics featured high densification with little cavities, suggesting the employed synthesis conditions were effective. XRD results indicated europium successful impregnated into the ABO_3 lattice but did not induce orthorhombic phase evolution. The dielectric properties elevated, dielectric frequency dispersion receded, diffused phase transition deteriorated, piezoelectric properties were enhanced, and ferroelectric properties elevated with a small addition of x ($< 0.45\%$), suggesting europium could evidently modify electrical properties of the ceramics. The optimal electrical properties (d_{33} = 384 pC/N, Q_m = 92, and k_p = 0.36) of the ceramics were detected at x = 0.45%.

ACKNOWLEDGEMENTS

This work was supported by the Henan Provincial Department of Science and Technology Research Project (172102210457), Nanhu Scholars Program for Young Scholars of XYNU, and the College Student Research Project of XYNU (2017-DXS-62). The authors sincerely thank Open Sharing Platform for Large Equipment of Xinyang Normal University.

REFERENCES

1. B. Jaffe, R.S. Roth, and S. Marzullo, *J. Appl. Phys.* 25, 809 (1954).
2. T.R. Shrout and S. Zhang, *J. Electroceram.* 19, 113 (2007).
3. W. Liu and X. Ren, *Phys. Rev. Lett.* 103, 257602 (2009).
4. D.S. Keeble, F. Benabdallah, P.A. Thomas, M. Maglione, and J. Kreisel, *Appl. Phys. Lett.* 102, 092903 (2013).
5. M. Tanmoy, R. Guo, and A.S. Bhalla, *J. Am. Ceram. Soc.* 91, 1769 (2008).

6. Y. Pu, M. Yao, H. Liu, and T. Frömling, *J. Eur. Ceram. Soc.* 36, 2461 (2016).
7. Z. Sun, L. Li, H. Zheng, and L. Luo, *Ceram. Int.* 42, 12246 (2016).
8. H. Yang, F. Yan, G. Zhang, Y. Lin, and F. Wang, *J. Alloys Compd.* 720, 116 (2017).
9. X. Chen, X. Ruan, K. Zha, X. He, J. Zeng, Y. Li, L. Zheng, C.H. Park, and G. Li, *J. Alloys Compd.* 632, 103 (2015).
10. R. Hayati, M.A. Bahrevar, T. Ebadzadeh, V. Rojas, N. Novak, and J. Koruza, *J. Eur. Ceram. Soc.* 36, 3391 (2016).
11. J. Wu, W. Mao, Z. Wu, and Y. Jia, *Mater. Lett.* 166, 75 (2016).
12. I. Coondoo, N. Panwar, H. Amorín, V.E. Ramana, M. Algueró, and A. Kholkin, *J. Am. Ceram. Soc.* 98, 3127 (2015).
13. Z. Wang, W. Li, R. Chu, J. Hao, Z. Xu, and G. Li, *J. Alloys Compd.* 689, 30 (2016).
14. P. Du, L. Luo, W. Li, Q. Yue, and H. Chen, *Appl. Phys. Lett.* 104, 152902 (2014).
15. D.I. Bilc and D.J. Singh, *Phys. Rev. Lett.* 96, 147602 (2006).
16. D.K. Patel, B. Vishwanadh, V. Sudarsan, and S.K. Kulshreshtha, *J. Am. Ceram. Soc.* 96, 3857 (2013).
17. R.A. Eichel, E. Erünal, P. Jakes, S. Körbel, C. Elsässer, H. Kungl, J. Acker, and M.J. Hoffmann, *Appl. Phys. Lett.* 102, 242908 (2013).
18. H. Sun, S. Duan, X. Liu, D. Wang, and H. Sui, *J. Alloys Compd.* 670, 262 (2016).
19. Y.S. Tian, Y.S. Gong, D.W. Meng, and Y.J. Li, *J. Mater. Sci.* 50, 6134 (2015).
20. Y.S. Tian, Y.S. Gong, Z.L. Zhang, and D.W. Meng, *J. Mater. Sci. Mater. Electron.* 25, 5467 (2014).
21. J. Wu, D. Xiao, W. Wu, Q. Chen, J. Zhu, Z. Yang, and J. Wang, *J. Eur. Ceram. Soc.* 32, 891 (2012).
22. L. Dong, D.S. Stone, and R.S. Lakes, *J. Appl. Phys.* 111, 084107 (2012).
23. K.W.P. And, Y.E. Sung, S. Han, A.Y. Yun, and T. Hyeon, *J. Phys. Chem. B* 108, 939 (2004).
24. M. Park and J.Y. Yoo, *J. Electron. Mater.* 41, 3095 (2012).
25. M. Jiang, Q. Lin, D. Lin, Q. Zheng, X. Fan, X. Wu, H. Sun, Y. Wan, and L. Wu, *J. Mater. Sci.* 48, 1035 (2013).
26. S. Ye, J. Fuh, L. Lu, Y.I. Chang, and J.R. Yang, *RSC Adv.* 3, 20693 (2013).
27. D. Fu, M. Itoh, S.Y. Koshihara, T. Kosugi, and S. Tsuneyuki, *Phys. Rev. Lett.* 100, 227601 (2008).
28. H.S. Kim, H.M. Christen, M.D. Biegalski, and D.J. Singh, *J. Appl. Phys.* 108, 054105 (2010).
29. W. Liu, J. Wang, X. Ke, and S. Li, *J. Alloys Compd.* 712, 1 (2017).
30. B. Qu, H. Du, and Z. Yang, *J. Mater. Chem. C* 4, 1795 (2016).
31. Y.S. Tian, S.Y. Li, Y.S. Gong, D.W. Meng, J.P. Wang, and Q.S. Jing, *J. Alloys Compd.* 692, 797 (2017).
32. R.K. Mishra, D.K. Pradhan, R.N.P. Choudhary, and A. Banerjee, *J. Magn. Magn. Mater.* 320, 2602 (2008).
33. R. Rani, S. Singh, J.K. Juneja, K.K. Raina, and C. Prakash, *Ceram. Int.* 37, 3755 (2011).
34. W. Wang, L.D. Wang, W.L. Li, D. Xu, Y.F. Hou, and W.D. Fei, *J. Alloys Compd.* 624, 284 (2015).
35. X. Tang, K.H. Chew, and H. Chan, *Acta Mater.* 52, 5177 (2004).
36. A.A. Bokov and Z.G. Ye, *J. Mater. Sci.* 41, 31 (2006).
37. J. Hao, W. Bai, and W. Li, *J. Am. Ceram. Soc.* 95, 1998 (2012).
38. X. Chao, Z. Wang, Y. Tian, Y. Zhou, and Z. Yang, *Mater. Res. Bull.* 66, 16 (2015).
39. P. Zhou, B. Zhang, L. Zhao, and L. Zhu, *Ceram. Int.* 41, 4035 (2015).
40. J. Wu, Z. Wu, W.J. Mao, and Y.M. Jia, *Mater. Lett.* 149, 74 (2015).
41. T. Badapanda, S. Sarangi, B. Behera, S. Parida, S. Saha, T.P. Sinha, R. Ranjan, and P.K. Sahoo, *J. Alloys. Compd.* 645, 586 (2015).
42. M.C. Ehmke, J. Daniels, J. Glaum, M. Hoffman, J.E. Blendell, and K.J. Bowman, *J. Am. Ceram. Soc.* 96, 2913 (2013).
43. E.E. Shafee and S.M. Behery, *Mater. Chem. Phys.* 132, 740 (2012).
44. E.K. Akdoğan, K. Kerman, M. Abazari, and A. Safari, *Appl. Phys. Lett.* 92, 112908 (2008).
45. Y. Saito, H. Takao, T. Tani, T. Nonoyama, K. Takatori, T. Homma, T. Nagaya, and M. Nakamura, *Nature* 432, 84 (2004).
46. S.W. Zhang, H.L. Zhang, B.P. Zhang, and G.L. Zhao, *J. Eur. Ceram. Soc.* 29, 3235 (2009).
47. A. Srinivas, R.V. Krishnaiah, V.L.N. Iranjani, S.V. Kamat, T. Karthik, and S. Asthana, *Ceram. Int.* 41, 1980 (2015).